scientific reports

Check for updates

OPEN

The efficient chitosan–polythiophene–graphene oxide bionanocomposite with enhanced antibacterial activity, dye adsorption ability, mechanical and thermal properties

Mohammad Amin Sedghamiz[1]✉, Mohammadhadi Mehrvar[2], Mohammad Amin Tavakkoli[3], Mehdi Sharif[2]✉ & Mehdi Sahami[4]

Water pollution is the most serious environmental issues due to toxic impurity such as dye and pathogenic microorganisms. The main goal of the present study is to produce a novel ternary chitosan–polythiophene–graphene oxide (CS–PTh–GO) bionanocomposites using the intercalation of GO into CS through solution mixing process followed by the in-situ polymerization of thiophene for removal of dye and killing microorganisms from an aqueous solution. The fabricated CS–PTh–GOs were characteristically examined via FTIR, XRD, SEM, TEM, TGA, tensile analysis and subsequently applied for adsorption of cationic dyes such as methylene blue (MB) in the dark or under light and killing the growth of Gram-positive and Gram-negative microorganisms. The data revealed that presence of PTh–GO enhanced the surface roughness, tensile strength, thermal stability, adsorption characteristics and antibacterial activity. The CS–PTh–GO showed 97% dye removal of MB in 50 min. Ultimately, the CS–PTh–GO bionanocomposites analysis against the growth of *Staphylococcus aureus*, and *Escherichia coli* manifesting a minimum inhibitory concentration (MIC) of 5 µg/mL, respectively. Thus, the CS–PTh–GO bionanocomposite has the potential to use as an efficient adaptable antimicrobial and dye absorbent of organic dyes in industrial wastewater.

Keywords Antimicrobial activity, Dye adsorption, Chitosan, Methylene blue, Bionanocomposite

In the recent years development of bionanocomposites has become a global that must be investigated to find their safety for ecological propose and human health at the environmental and organism levels[1,2]. The modern technology in printing and dyeing have enhanced quality of life, but wastewater from the industry led to water pollution, endangering social progress[3]. Certain dyes also, can be harmful to plants and animals, as they may contain toxic compounds which are water-insoluble and non-biodegradable[4–6]. Dye removal from water accomplished using different physical, chemical, and biological technologies. These techniques included filtration via adsorption membrane[7], coagulation-flocculation[8], electrochemical[9] and biological technology[10]. It is well known that physical adsorption techniques is an effective technology for treating of water due to it simple operation, cost-effectiveness and flexibility in design as well as not producing subsidiary pollutants product[11]. A number of adsorbent derived from various organic or inorganic sources applied to remove dyes from water, including carbon active[12], graphene-based adsorbents[13], biopolymers[14] and nanocomposites[15,16]. In last decades the bio-based materials and their nanocomposites have become more popular due to their economic advantage and degradability[17]. Bio-polymer based nanocomposites with enhanced properties were produced using modified nanomaterial's embedded in the polymeric matrix that are able to combine the unique

[1]Department of Chemical, Petroleum and Gas Engineering, Lamerd Higher Education Center, Shiraz University of Technology, Lamerd, Iran. [2]Department of Polymer Engineering, Shiraz Branch, Islamic Azad University, Shiraz, Iran. [3]Faculty of Mechanical Engineering, University of Isfahan, Isfahan 81746-73441, Iran. [4]Department of Mechanical Engineering, The University of Akron, 244 Sumner Street, Akron, OH 44325-3903, USA. ✉email: sedghamiz.ma@gmail.com; mehdi.sharif.iau@gmail.com

properties of both filler and polymer components using a synergistic effect[18,19]. Different applications were undertaken using bionanocomposites included removing of dye from wastewater, antibacterial and delivering drugs, etc. Moreover, the existence of microbial pollutions in drinking water represents a remarkable danger to human health and cause many infectious diseases[20]. Therefore, fabrication of a high performance adsorbent with high-removal efficiency for microorganisms is an attractive technology. Thus, biopolymer-based adsorbents are unique method in the adsorption of pollutants from water[21] Elella et al. synthesized adsorbent hydrogels with high swell ability near ~ 911% and observed that the maximum adsorption capacity was 93.5% (166.7 mg/g) in the basic pH condition[9]. In another research Elella and coworkers produced an antimicrobial gelatin based hydrogels for wastewater treatment. They found that synthesized gelatin based hydrogels have the superior antimicrobial activity and also very promising adsorbent for capture of Cu ions from aqueous solution[22]. Biopolymers such as chitosan (CS) have amine ($-NH_2$), hydroxyl (–OH) and ionic functional groups which can react with dye molecules using electrostatic attraction and hydrogen bonds interaction and also biological[18,23,24]. The amine groups of CS also have positive charge that electrostatically react with the negative charge of the microbial membrane led to antimicrobial efficiency and dye removal ability[19,25–27]. Besides, chemical or physical modification procedure of chitosan such as surface modification and mixing with nanoparticles led to more antimicrobial and dye removal property[28,29].

In these years nanomaterials such as silver nanoparticles, SiO_2, TiO_2, clay, graphene and its derivate has attracted great attention due to their broad application and effective dye adsorbents and antibacterial performance[30–32]. Motshabi et al. reported that presence of TiO_2 nanoparticles affected the maximum adsorption capacity of adsorbents for removing MB dye in locust bean gum (LBG) hydrogel at neutral pH.[33] Abu Elella et al. fabricated xanthan gum-SiO_2 nanocomposites adsorbent with highly antibacterial efficiency. They applied it as a filter for adsorbent of MG dye and killing the Gram+and Gram− bacterial strains[10]. Benhalima et al. developed bionanocomposite containing silver nanoparticle-functionalized zeolite applied it as catalysts for hydrogenation of dye. They observed good catalytic ability of bionanocomposite for the hydrogenation of DR16 in various real-life with a high efficiency (99%)[34]. Benhalima and coworkers produced novel bionanocomposite hydrogels and used it for the removal of highly toxic basic red and MB cationic dyes. They found that presence of AgZ in the cellulose based hydrogels led to production of bionanocomposite hydrogels with significantly enhanced adsorption capacity, antimicrobial activity and thermal stability[35]. Abu Elella et al. prepared gelatin based nanocomposites adsorbent by incorporating nanoclay for removal of malachite green (MG) dye. From adsorption experiments and isotherm modeling they found that the fabricated nanocomposite adsorbent had a maximum adsorption capacity of 950.5 mg/g using 350 mg/L of MG dye at pH 9 within 45 min[36]. Ferfera-Harrar synthesized carboxymethyl cellulose/gelatin/citrate@Fe3O4 magnetite bionanocomposites and used it in adsorption and photocatalytic degradation of pharmaceutical pollutants[37]. They also produced bioadsorbents hydrogel containing montmorillonite. From adsorption results, they found that the presence of 2 wt% clay improved adsorption capacity from 1685 to a highest value of 1749 mg/g[32]. Graphene oxide (GO) is an oxide form of graphene, which has oxygen functional groups on its planar surface[13,38–40]. Recently, research has focused on the antibacterial and dye removal properties of GO and its nanocomposite[41–43]. Researchers reported that the anti-bacterial performance of GO related to the reaction of functional groups of GO with bacteria cell via chemical or physical interactions[44]. Carpio et al. studied the antimicrobial effect of GO that modified with silanol groups and observed that the membrane stress induced via sharp edge of GO nanosheet led to integrity of bacterial membrane decreased and RNA leakage[45]. The GO-CS bionanocomposite MB-dye adsorbents developed and their dye removal efficiency were investigated in litarature[46–48].

Conductive polymers (ICPs) are a special kind of synthesized polymers that are inherently conductive. They have the characteristics of polymers and the semiconductors and applied in actuators, biomedical, catalysts, energy storages, electric device, and also water purification[49–51]. Among ICPs, the one main famous candidate is polythiophene (PTh). Although ICPs are biocompatible but their adsorption capacity is not significantly high[52]. However, combination of IPNs with nanomaterials led to formation of nanocomposite with a high adsorption capacity[53]. PTh has some advantage such as high chemical and environmental stability, not expensive and highly electrically conductivity and used in various applications[54–58]. Mir et al. synthesized conducting polymer (CP)-based biocomposite hydrogels for application as drug delivery vehicles. They observed that fabricated hydrogels have a slow drug release rate of about 10 h due to the presence of the conducting polymer[59]. Myrick et al. prepared polythiophene-graphene oxide (GO) and applied it for antibacterial agent and visible light photocatalyst. They observed that GO-PTh has higher degradation efficiency compared to pure PTh[60]. Benhalima et al. produced cellulose based composite hydrogels containing conductive polymer (PANI) and inorganic filler for removal of crystal violet and acetamiprid pollutants. They observed that the presence of TiO2-PANI led to better photocatalytic activity with an almost complete removal (99%) of dye in 80 min of solar light[61]. The composites of chitosan and conductive polymers are studied for broad range of applications. Chitosan-PANI composites were made to remove dye under UV light[62]. Ceiba pentandra fibers coated with PANI molecules for methyl orange degradation[63]. Mohammadi et al. studied the effect of polyaniline on the antibacterial and mechanical properties of CS-PANI films[64,65]. Moutsatsou et al.[66] fabricated antibacterial PANI/chitosan nanofibrous membranes for wound dressing. Pandiselvi et al. prepared CS-PANI-ZnO bionanocomposite to remove dyes with high efficiency[67]. They found that the maximum dye removal were 88.5% for MB blue with PZO/chitosan amount of 0.3 g/L and neutral pH in 120 min of sunlight exposure.

Due to the literature study, it is found that there is only scarce information about the investigation of conductive polymer and graphene oxide hybrids filler concentration and its interaction on the properties of chitosan based biopolymer nanocomposites. Therefore, the present paper aim to fabricate high-performance ternary bionanocomposites eith ehnaced mechanical and thermal properties for removing of MB dye with antibacterial activity based on chitosan, polythiophene and graphene oxide using a simple two-step method. In the first step, the GO filler was incorporated whitin CS using solution mixing. In a second step, thiophene

monomer synthesized in the presence of CS–GO to produce CS–PTh–GO bionanocomposites. The chemical structure, morphology and properties of the fabricated materials were investigated using SEM, TEM, FTIR, XRD, Tensile and TGA analyses and inhibition the growth of several pathogenic microorganisms and dye removal efficacy also investigated. This novel bionanocomposite exhibits dye removal ability and long-lasting antibacterial activity at low content and also photocatalytic performance.

Experimental

Materials

Graphene oxide produced from graphite powder (powder (< 50 μm) from Merck-Germany) using the method described in the previous paper[68]. Thiophene monomer, acetonitrile, $Fecl_3$, MB and Chitosan (CS) (Mw = 100,000–300,000, DA ≥ 80%) were obtained from Sigma-Aldrich, Germany and used as received without any purification.

Preparation of CS–GO bionanocomposite

For production of the CS–GO bionanocomposite 0.20 g of CS dispersed in 200 mL 1% acetic acid solution and magnetic stirred for 2 h. 0.30 g of GO was dissolved in 40 mL deionized water and mixed for 4 h. Then the above suspension added to CS solution and sonicated for 10 min. At end of this time, the product collected and dried at 60 °C (Fig. 1a).

CS–PTh–GO bionanocomposite production

CS–PTh–GO bionanocomposite were prepared by interfacial polymerization method at different weight ratio of thiophene to GO (1:10, 1:15 and 1:20 called TG1, TG2 and TG3)[69]. At first, the required amount of synthesized CS–GO was dissolved in 40 mL of water using an ultrasonic Homogenizer and mixed for 20 min. Then $FeCl_3$ was added to the CS–GO solution and mixed for 1 h (the molar ratio of thiophene monomer to $FeCl_3$ was 1:4). After than it the thiophene monomer that dissolved in *n*-hexan was added slowly into the above solution and kept mixing via magnetically stirrer at room temperature for 24 h. finally the products were collected with centrifugation at 10,000 rpm, washed 3 time with ethanol and dried at 50 °C for 10 h. PTh and PTh–CS were also prepared using the abovementioned method (Fig. 1b). Moreover, after washing the resultant solution casted into petri dish and drying to produce a film with 50 μm thickness.

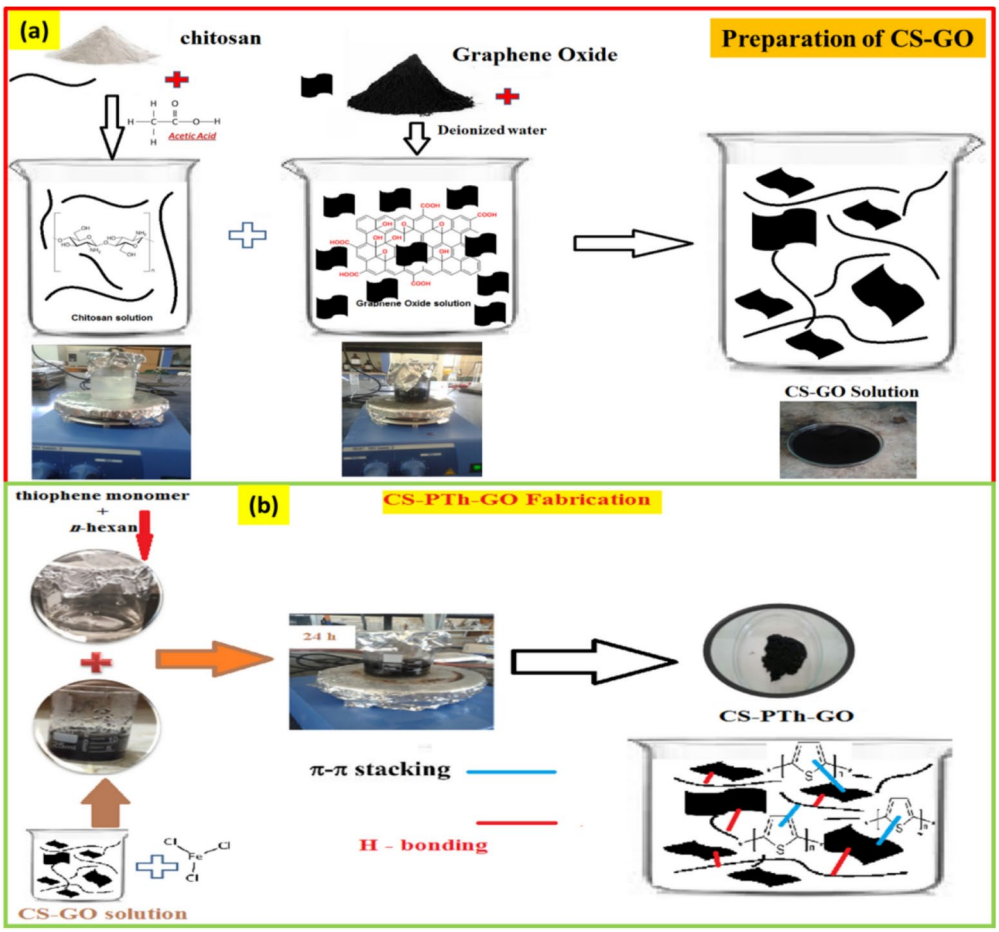

Fig. 1. A schematic steps for the preparation of CS–GO and CS–PTh–GO bionanocomposites.

Characterization

X-ray diffraction test (XRD, STOE STADIMP, Germany) was applied to study the crystalline structure of bionanocomposites under Cu Ka irradiation. FTIR analysis was used to detect the chemical structure of samples. Scanning electron microscope (SEM, Hitachi S-2300) and Transmission electron microscopy (TEM) were used to observe the dispersion and deposition of PTh on GO surface and into the CS matrix (TEM Leo 910). Absorption spectrum was recorded with a UV–Vis spectrophotometer (2401 PC model; Shimadzu, Kyoto, Japan) in the wavelength range of 250–600 nm. The tensile properties of bionanocomposites were determined using an Instron Tester 6025.

The solution of dye (methyl blue) produced via the dispersion of 1000 mg MB in 1 L water. Batch experiment was applied for optimization of the parameters that affecting the adsorption of MB by the CS–PTh–GO bionanocomposites in the dark. 0.2 g of the adsorbents with desired amount of the 100 ml MB solution was taken in Erlenmeyer flasks for particular time period at 200 rpm. After an experiment time, the CS–PTh–GO bionanocomposites separated, and the concentration of MB present in the solution determined via UV–visible analysis at 580 nm. The amount of MB calculated using the following equation:

$$q_t = \frac{(C_0 - C_t)}{m}$$

$$\%Dyeremoval = \frac{C_0 - C_T}{C_T} \times 100$$

In this equation C_o and C_t *are* the MB concentration at t = 0 and t = experiment time in mol/L, and m = the CS–PTh–GO bionanocomposite mass (g).

The photocatalytic activity of samples was determined using degradation of MB in the radiation of tungsten lamp. The MB (0.1 and 0.05 g/L) dissolved in distilled water that contain 2 g/L of the bioadsorbent. Then, MB adsorption determined in the darkness for 60 min to reach equilibrium adsorption of MB for each sample. After this, the MB concentration determined using UV–visible analysis at 465 nm. Then, the solution was kept in the radiation of light for required experimental time and then withdrawn to estimate the concentration of MB. The percentage of MB removal at different exposure was calculated via the equation:

$$Degradeddye\,(\%) = 100 - \frac{C_0 - C_t}{C_t} \times 100$$

The antibacterial efficiency of bionanocomposites was investigated against Gram-positive and Gram-negative bacteria according to the method described in literature[70].

Results and discussion

FTIR analysis

The chemical structure of pure PTh, GO, CS and CS–PTh–GO bionanocomposite were studied by FTIR analysis and the results are shown in Fig. 2. In this figure it can be seen that the O–H stretching vibration of PTh located at 3440 cm^{-1} and the absorption bands of C–H groups of thiophene unit observed at 2875, 1630 and 1480 cm^{-1}[71]. The absorption peaks at 850 and 680 cm^{-1} are the characteristic vibrations peaks of C–S and also C–S–C of thiophene ring[69,72]. For GO the bands at 3420 cm^{-1}, 1727 cm^{-1}, 1060 cm^{-1}, 1410 cm^{-1} wavenumber related to the of hydroxyl, C=O, carboxyl and epoxide groups[55]. In the CS spectrum, the absorptions peak at 1650 and 1540 cm^{-1} demonstrated the existence of OH groups and vibration of C-NH_2[73]. The peaks in the range of 1150–1035 cm^{-1} are the stretching vibration of C–O–C bands. The characteristic band of C–N group appeared at 900 cm^{-1}[73,74]. In the CS–PTh–GO the shift in the peaks position at 690 cm^{-1} and 830 cm^{-1} of C–S and C–S–C of thiophene observed due to the π-π interaction between PTh and CS. In the spectrum of CS–PTh–GO the intensity of peak at 1727 cm^{-1} is lower compared to carboxyl groups of GO due to the hydrogen bond interaction between chitosan and the oxygenated functional groups of GO[75]. Moreover, a lower shift in the amide band of CS from 1540 to 1380 cm^{-1} confirms the involvement of chitosan's amine groups in hydrogen bonding with COOH groups of GO. It can also be seen that the hydroxyl peak is shifted from 3500 in pure CS to 3450 cm^{-1} CS–PTh–GO as a result of stronger H-bonding between CS and GO[75]. The suggested chemical structure of CS–PTh–GO and interaction between components is presented in scheme 1.

Microstructure observation

The X-ray analysis of CS and CS based bionanocomposites are shown in Fig. 3. The CS has the peaks at 2θ = 14° and a 22° confirmed its amorphous nature[76]. The x-ray pattern of CS–GO display diffraction peak in 5–15 region due to the agglomeration of GO palates due to the Van der Waals force interaction between GO layers. The crystalline peak of the GO shift to the lower angles with lower intensity in CS–PTh–GO biocomposite compared to CS–GO as a result of the diffusion of the CS chains into the GO gallery space during in-situ polymerization of PTh that led to interlayer space between GO increased[77]. Therefore, in the CS–PTh–GO bionanocomposite the successful exfoliation and uniformly dispersion of PTh–GO in the CS matrix occurred.

Figures 4 and 5 present the microscopic images of the chitosan based bionanocomposites particles and films at different magnifications. The CS–GO SEM image shows that the GO plates that aggregated with each other. In the CS–PTh–GO (Fig. 4e–f) there is not any agglomeration of GO and the PTh decorated GO better distributed in the chitosan matrix than GO. Moreover, it can be seen that the ratio of thiophene to GO affected the dispersion of GO in the CS matrix (Fig. 4e–f). GO possesses abundant oxygen-containing functional groups, such as hydroxyl (–OH), carboxyl (–COOH), and epoxy (–C–O–C) groups, which render its surface highly

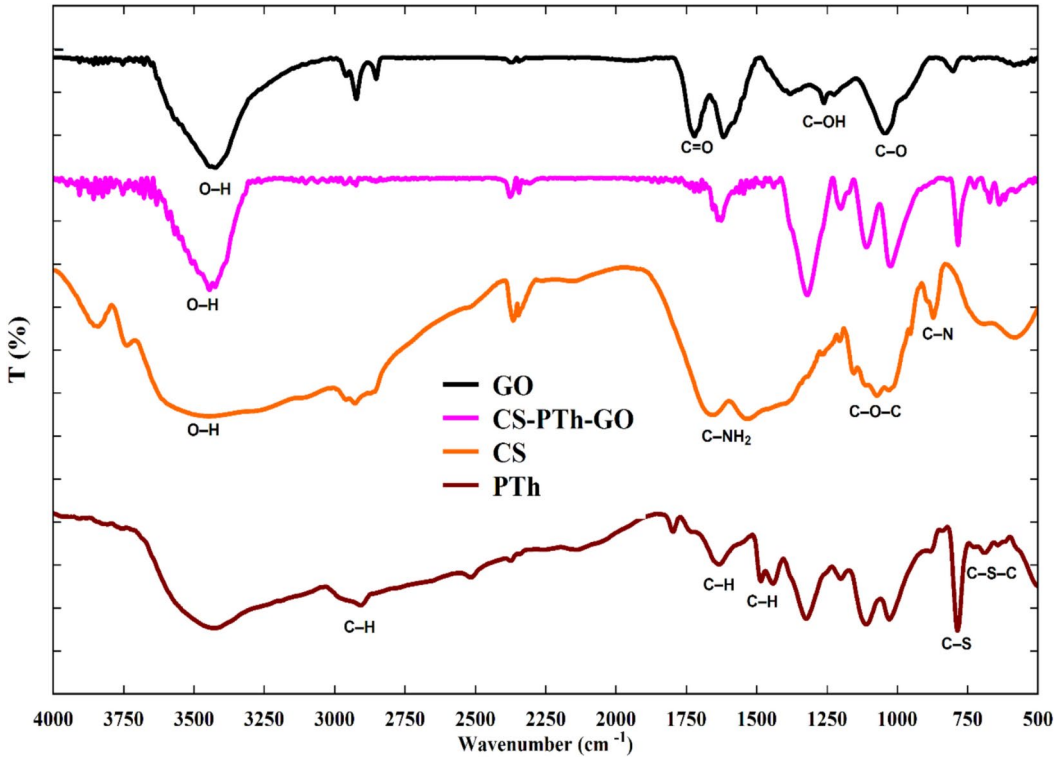

Fig. 2. FTIR spectrum of pure components and CS–PTh–GO bionanocomposite.

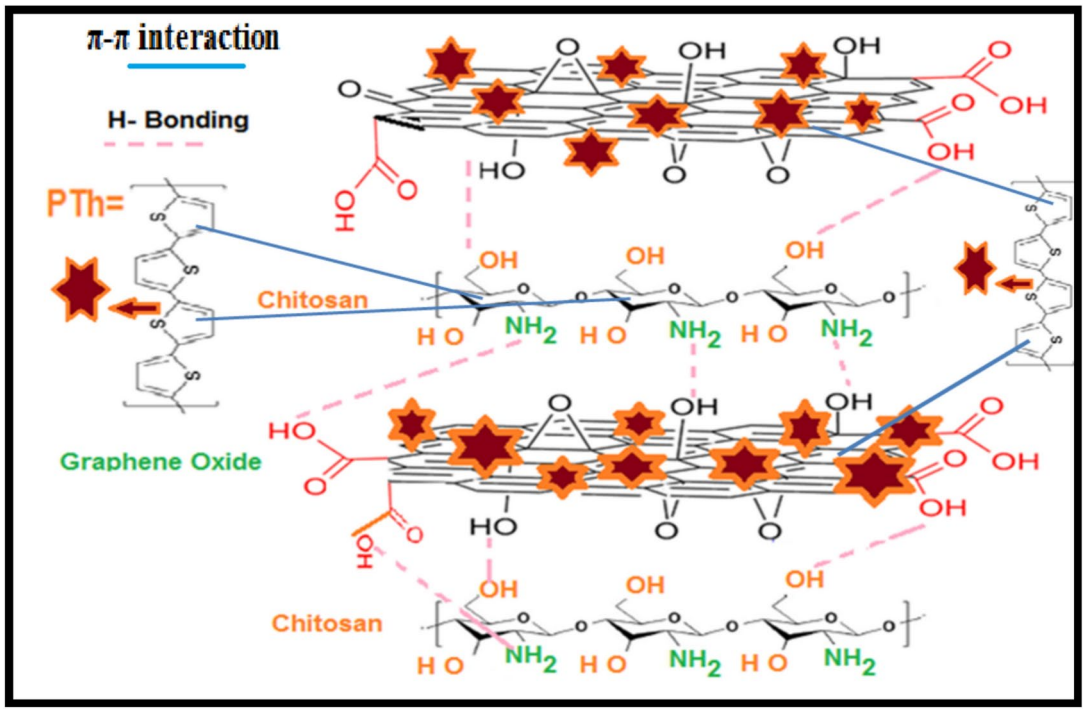

Scheme 1. Schematic Possible interaction between CS–PTh–GO components.

reactive. Chitosan has free amine (–NH2) and hydroxyl (–OH) groups along its backbone. The interactions between GO and chitosan occur primarily through the hydroxyl and carboxyl groups of GO form hydrogen bonds with the hydroxyl and amine groups of chitosan. The insitu polymerization of thiophene monomer led to deposition of PTh on the GO layer. When polythiophene deposited on the surface of GO, the CS chains better

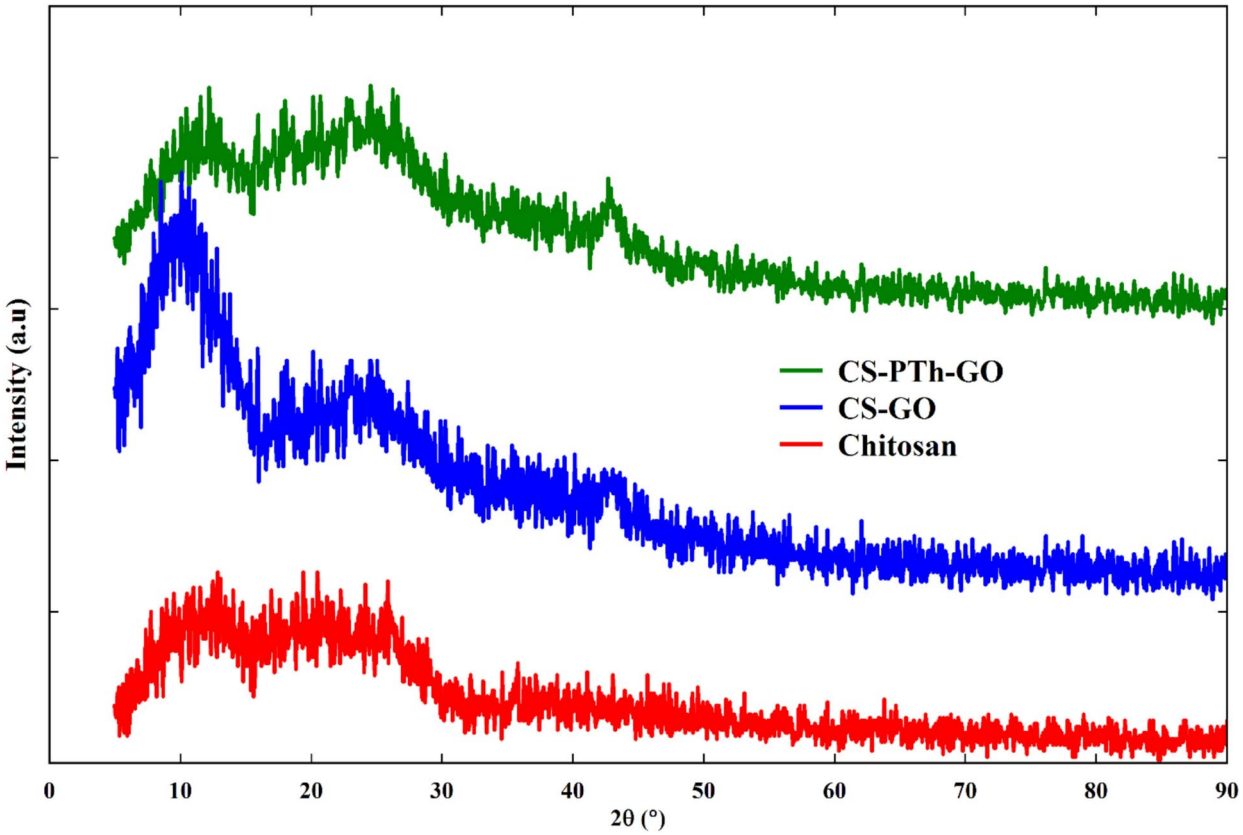

Fig. 3. X-ray analysis of CS, CS–GO and CS–PTh–GO bionanocomposite.

penetrated into the GO layer space and the interaction between functional groups of GO and CS increased. The interactions enable a uniform dispersion of GO within the chitosan matrix and reducing agglomeration. This results in a CS–PTh–GO nanocomposites with a more homogeneous and interconnected structure. However, it can be seen that when PTh and GO dispersed in the CS matrix the surface roughness of CS–PTh–GO increased compared to pure CS which are essentially helpful when applied as dye removal adsorbent.

The TEM (Fig. 5) images show the dispersion of GO and PTh–GO in the CS matrix. From TEM images it can be observed that in the CS–PTh–GO composite, GO layers decorated with PTh with ~ 50 nm size and modified GO better dispersed in the CS compared to pure GO. Deposition of PTh on the GO surface enhanced the interaction between CS chains and GO functionalized groups that led to production of 3D PTh–GO networks[51,69].

Dye removal efficiency

The dye adsorption efficiency of the CS–PTh–GO bionanocomposites at different time, pH and thiophene to GO ratio (PTGs) was analyzed to describe the performance of CS–PTh–GO as dye adsorbent. Figure 6 presents the cationic dye (MB) removal efficacy of the adsorption CS–PTh–GO bionanocomposite. From this figure it can be seen that, in the first 10 min, dye removed very rapidly and then reached to the equilibrium condition. The rapid increase in dye removal at the initial time related to the presence of more active site for adsorption of dye. But during adsorption process the active site decreased resulted to decrease in the rate of dye removal. The results show that the adsorption time for reach to equilibrium condition was about 50 min in PTG2 bionanocomposite. Figure 6 shows that the adsorbent nature (ratio of thiophene to GO), affected the removal efficiency and increased from 47 to 97% for CS–PTh–GO bionanocomposite. The presence of electrostatic interactions (π–π and electrostatic interactions), hydrogen bonds and electron sharing between the –NH, $–CONH_2$, –OH, $–NH_3^+$, $–CO_2H$, and –COO groups evolve during MB adsorption[78]. MB's nitrogen atoms lone pairs and hydroxyl groups of PTh–GO–CS interacted via H-bond. Therefore, MB molecules' ideally planar configuration and the abundance of aromatic rings in CS–PTh–GO nanocomposite and the π-π stacking interactions could occur between MB molecules and CS–PTh–GO nanocomposite. Moreover, MB adsorption occurs due to the electrostatic interaction of the negatively charged carboxyl groups of GO and positively charged dye molecules. The –OH and –NH2 groups present in CS polysaccharide and GO layers, as well as the aromatic rings in MB molecules and PTh, interact by the Yoshida H-bonding mechanism. Moreover, the high adsorption capacity of CS–PTh–GO nanocomposite was also ascribed to π–π and electrostatic interactions between PTh and MB[79]. The high removal capacity of CS–PTh–GO (PTG2) bionanocomposite confirms its high affinity for the removal of MB dye from the solution.

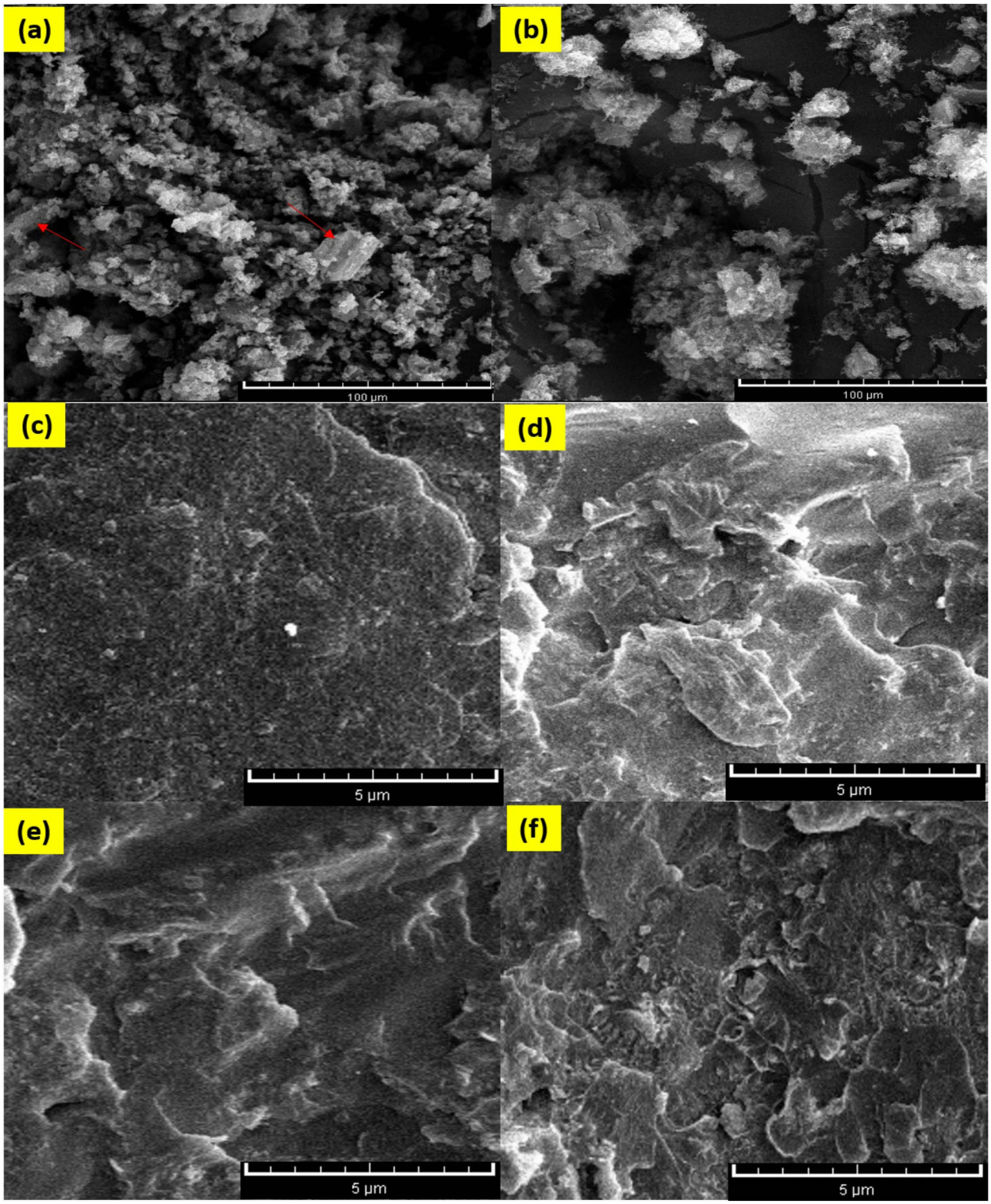

Fig. 4. The SEM analysis of the CS based bicomposites: (**a**) CS–GO, (**b**) CS–PTh-–GO, (**c**) CS film, (**d**) CS–GO film, (**e**) CS–PTh–GO (PTG2) film and (**f**) CS–PTh–GO (PTG3) film.

Initial concentration of dye also affected the dye removal (%) which are presented in Fig. 7. It can be observed that at the lowest dye concentration (20 mg/L), the CS–PTh–GO bionanocomposite has the removal efficiency in the range of 97%. The improved removal of dye at the lower dye content can be related to the faster diffusion of the dye molecules on to the active sites of bionanocomposite[80]. But, at higher dye concentration, the removal rate of bionanocomposite decreased to 40% as a result of the movement of dye molecules into the active sites of CS–PTh–GO hindered with inter particle diffusion and steric repulsion force between the solid particles[81].

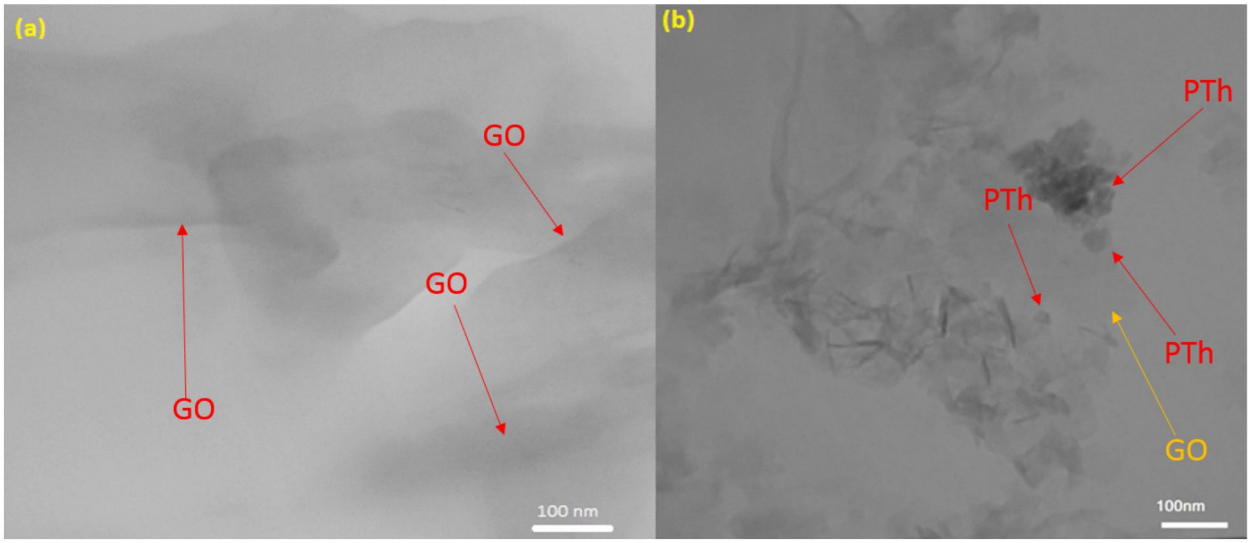

Fig. 5. TEM analyses of (**a**) CS–GO and (**b**) CS–PTh–GO (PTG2).

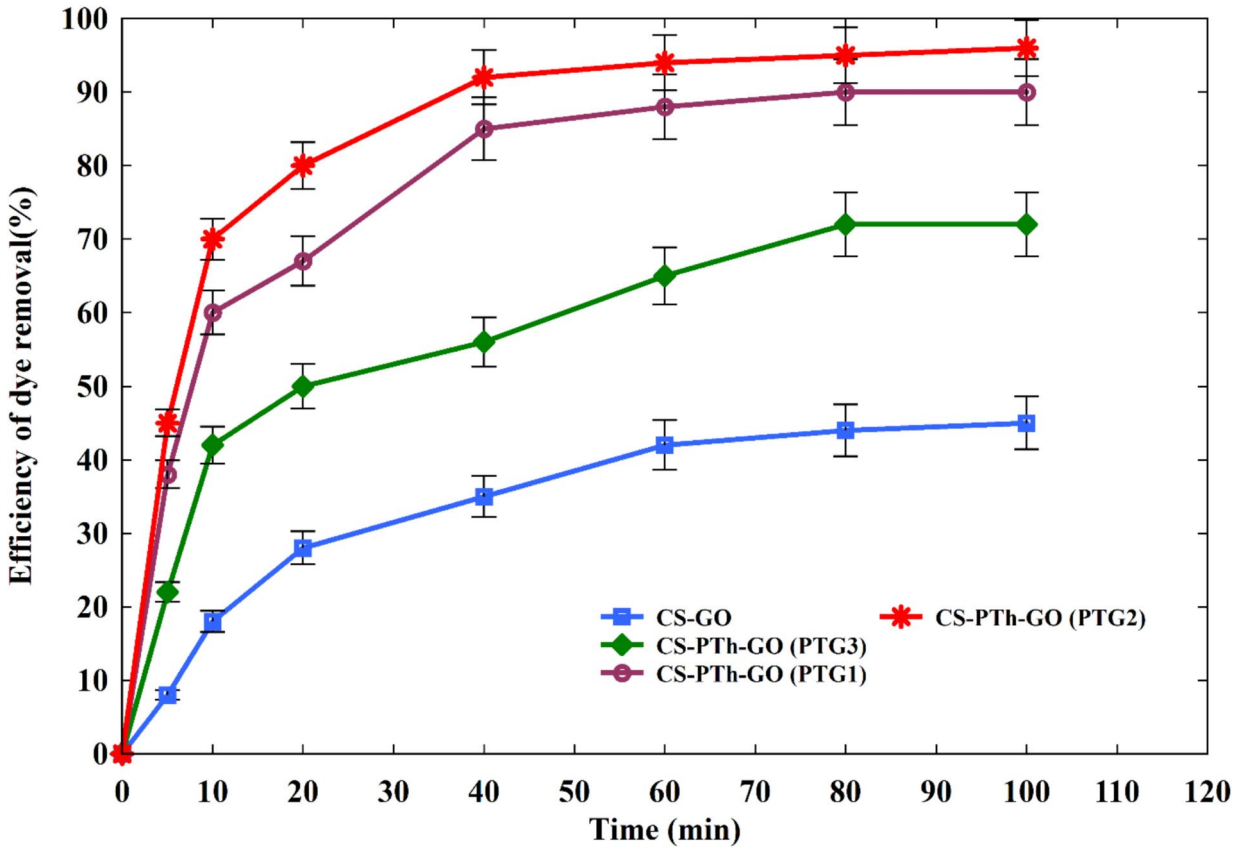

Fig. 6. Removal of dye for CS–GO and CS–PTh–GO bionanocomposite.

One of the main factors that affected the removal efficacy of adsorbent is the pH. The effect of pH on the adsorption of dye presents in Fig. 8. It is obviously observed that maximum removal efficiency is 98% at pH = 4. At lower pH amine and hydroxyl protonated that increase the electrostatic interaction between the positive charge of adsorbent and negative charge of dye led to higher dye removal ability. However, at high pH (6–9) presence of OH^- ions and deprotonations of groups reduced the electrostatic interactions between adsorbent and dye.

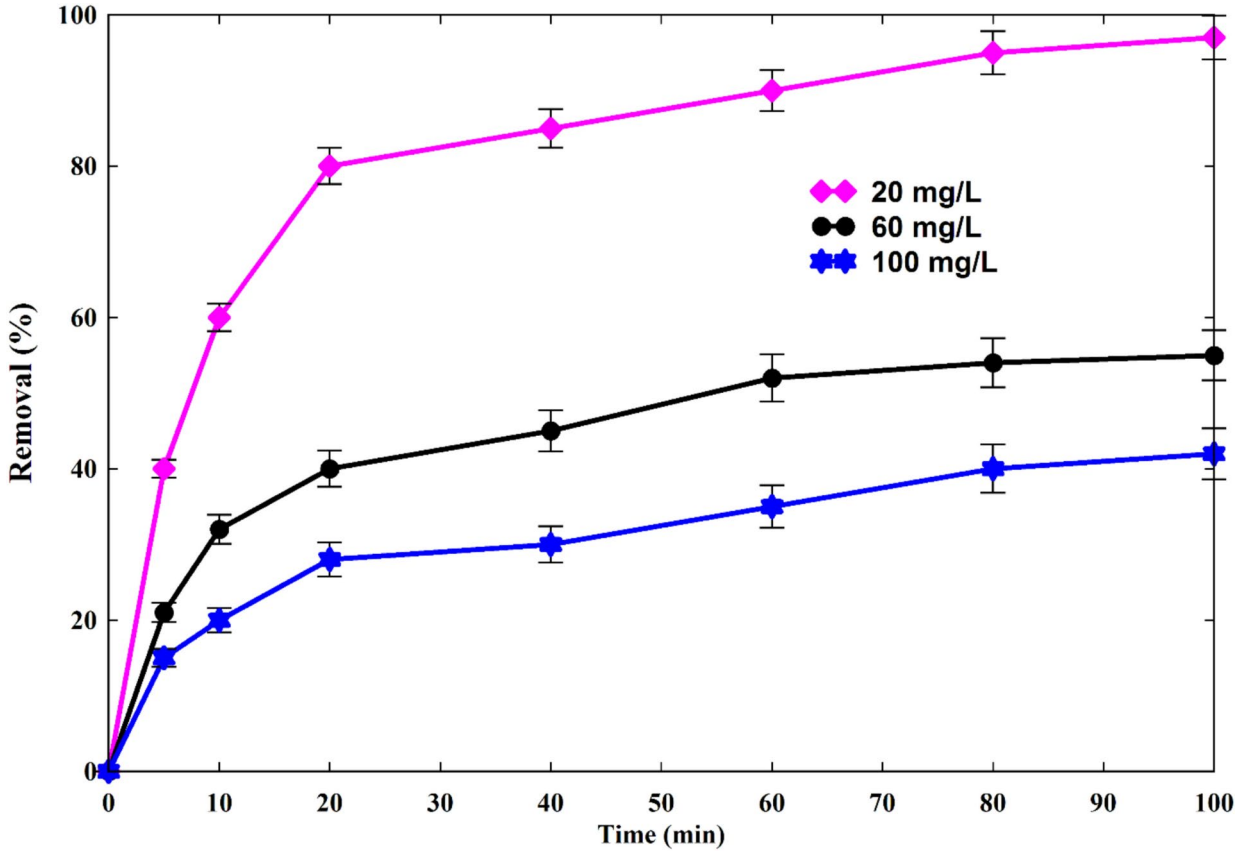

Fig. 7. The effect of dye concentrations on the removal efficiency CS–PTh–GO (PTG2).

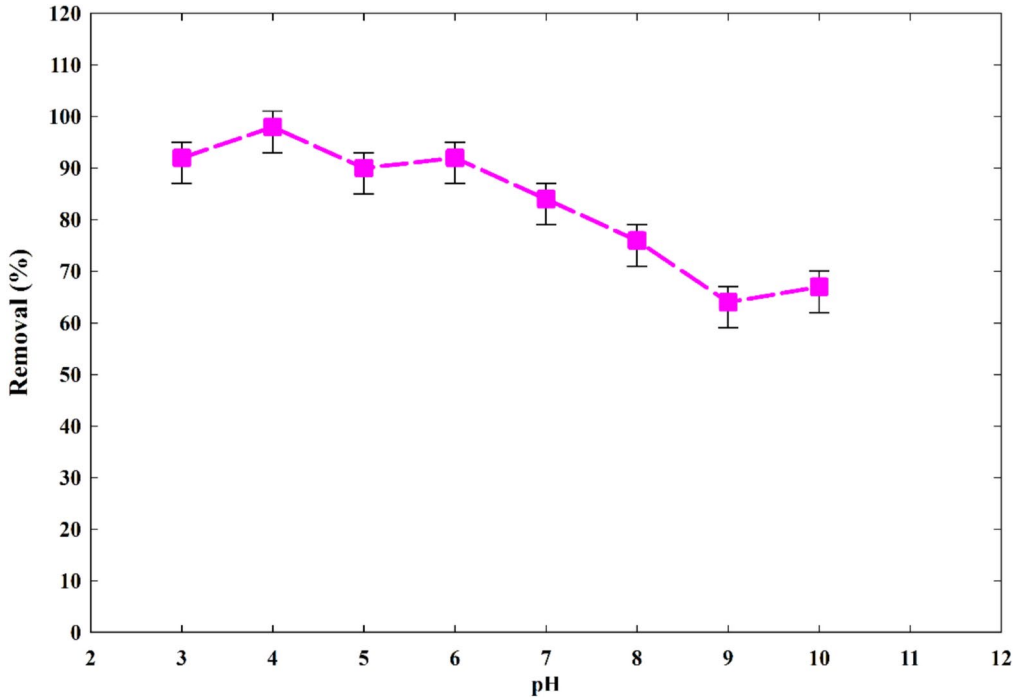

Fig. 8. Effect of pH on the dye removal efficiency for CS–PTh–GO (PTG1) bionanocomposite.

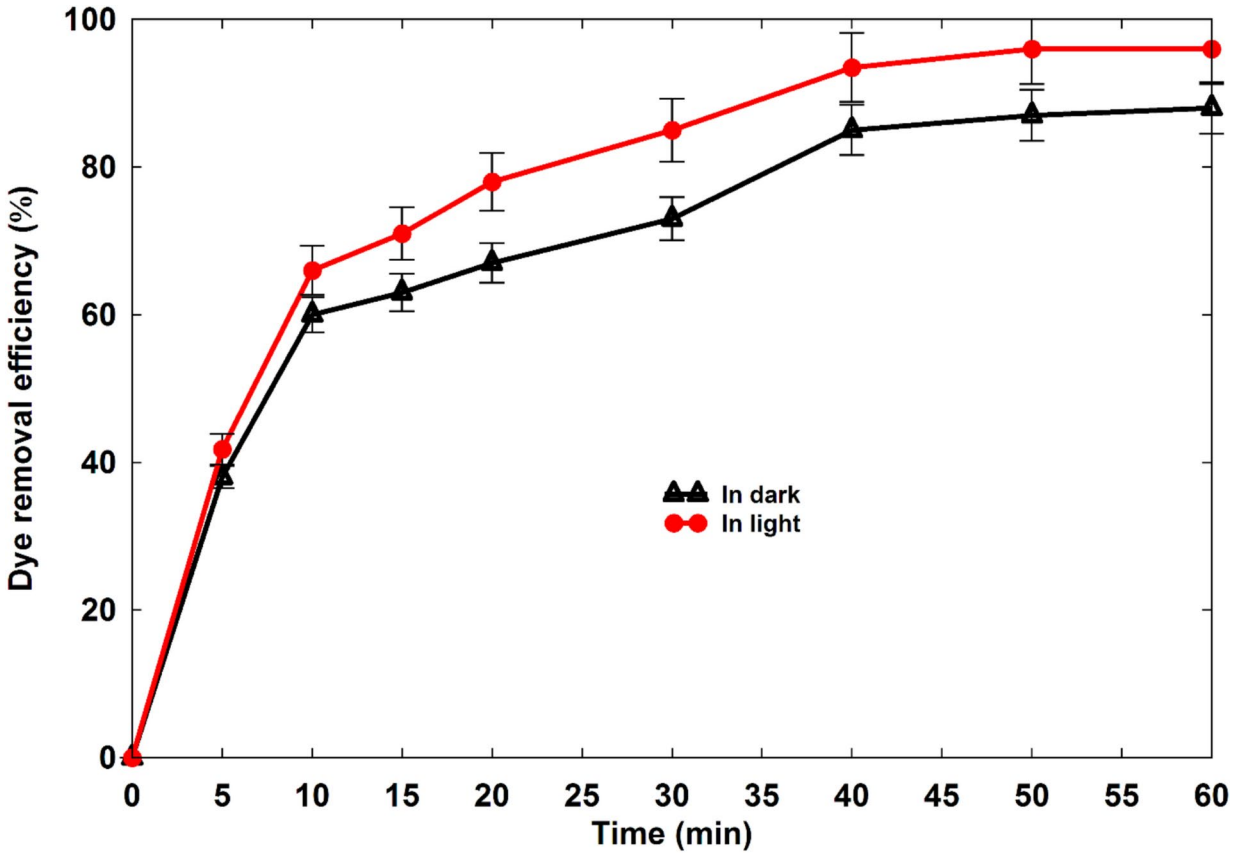

Fig. 9. photocatalystic activity of CS–PTh–CS in dark and light.

Adsorbent	Dye	pH	Time equilibrium (min)	Reference
Sulfonated Chitosan-montmorillonite	Methylene Blue	7	75	[82]
Magnetized chitosan nanocomposite	malachite green dye	7	180	[83]
Carboxy methyl Cellulose/chitosan/GO	cationic dyes	7	180	[84]
RGO@ZnO composite	Rhodamine B	7	120	[85]
Hydrogels/magnetic-GO nanocomposite	Malachite green	7	120	[86]
MOF nanocomposite	Methylene blue	7	260	[87]
PGS–CS–GO	Methylene blue	7	300	[88]
Chitosan–Montmorillonite/PANI nanocomposite	Methylene blue	7	120	[89]
PANI/GO	Methylene blue	7	270	[90]
Phytic acid doped polyaniline nanofibers	Methylene blue	7	60	[91]
CS–PTh–GO	Methylene blue	7	50	This study

Table 1. Comparison of CS–PTh–GO bionanocomposite with other reported adsorbents.

The photocatalystic ability was studied using the irradiation on CS–PTh–GO to understand the photocatalytic activity of CS–PTh–GO bionanocomposite and the results are shown in Fig. 9. For this propose two different experimental conditions. In the first one, the removal ability of bionanocomposite in dark place studied and determined removal efficiency was 78.6% and at the other condition (light) CS–PTh–GO has the efficacy of 95.1%.

Comparison with other adsorbent

The fabricated CS–PTh–GO binanocomposite compared with the other adsorbents synthesized by reserachers and reported in the literature and presented in Table 1. It is concluded that CS–PTh–GO possess good tendency in terms of MB removal. The synthesized CS–PTh–GO binanocomposite has the same range of equilibrium

dye removal time compared to the reported adsorbent. Thus the prerpared CS–PTh–GO binanocomposite is a competent bioadsorbent for the removal of cationic dyes like MB from the waste water.

Adsorption mechanism of dye

FTIR analysis was used for the better understanding the adsorption mechanism of dye CS–PTh–GO nanocomposites and the results are presented in Fig. 10. After MB dye adsorption, the broad band's at 3500 cm^{-1} was observed due to the hydrogen bond between the CS–PTh–GO nanocomposites and the electronegative nitrogen atoms in the MB molecular structure. The decrease in the intensity of peak 1650 cm^{-1} for CS–PTh–GO–MB compared to CS–PTh–GO related to the electrostatic attraction of MB dye molecules with CS–PTh–GO nanocomposites. The appearance of a strong peak s at 1500–1390 cm^{-1} in the FTIR spectrum of the CS–PTh–GO–MB related to the C–H stretching of CH_3 groups in the MB molecular structure[92,93]. Scheme 2 shows the possible absorption mechanisms between CS–PTh–GO and MB dye.

Anti-bacterial efficiency of the CS–PTh–GO biocomposites

The antibacterial ability of CS–PTh–GO biocomposites was investugated usingthe minimum of inhibitory content (MIC) study against Gram-positive and Gram-negative microorganisms (Table 2). The results demonstrated that CS–PTh–GO inhibited the growth of bacteria at minimum concentration lower of 5 µg/mL, but, CS–GO and CS–PTh, showed minimum inhibitory activity at higher concentration. CS has a positive charge surface and attached to the negative charge of bacterial surface led to altered membrane permeability, which results in leakage of intracellular constituents causing cell death[94]. The antibacterial activities of GO-based materials are attributed to their dispersion, size, and oxidization capacity[41]. Three-step cytotoxicity mechanisms have previously proposed for carbon based nanoparticles. The first step is bacterial adhesion or deposition onto nanoparticles resulting in direct bacterium- nanoparticle contact. The second step is that nanoparticles would make intimate, membrane disruptive interaction with bacteria, inducing membrane stress. The third step involves disrupting a specific microbial process by disturbing or oxidizing a vital cellular structure or component. In general, the dispersion of GO depends on functional groups on GO sheets and their interaction with matrix. Deposition of PTh on GO surface causes the carboxyl, hydroxyl, and epoxy groups on GO sheets form much more active and GO can form more stable dispersions in CS matrix compared to pure GO and PTh, as observed in morphological observation section, thus offers more opportunities to interact with cells for cell deposition[22]. Gram-negative bacteria such as *E. coli* cells may first deposit on GO during incubation[95]. Moreover, the higher enzymatic activity induced by GO to Gram-negative bacteria such as *E. coli* concluded that the sharp edges of GO allowing it to easily penetrate through *E. coli's* thin peptidoglycan layer[96,97]. Akhavan et al. performed a series of experiments to demonstrate the behavior of *E. coli* bacteria in the presence of GO. They showed that GO nanosheets with oxygen-containing functional groups can better trap the bacteria compared to graphene nanosheets with reduced functional groups[45].

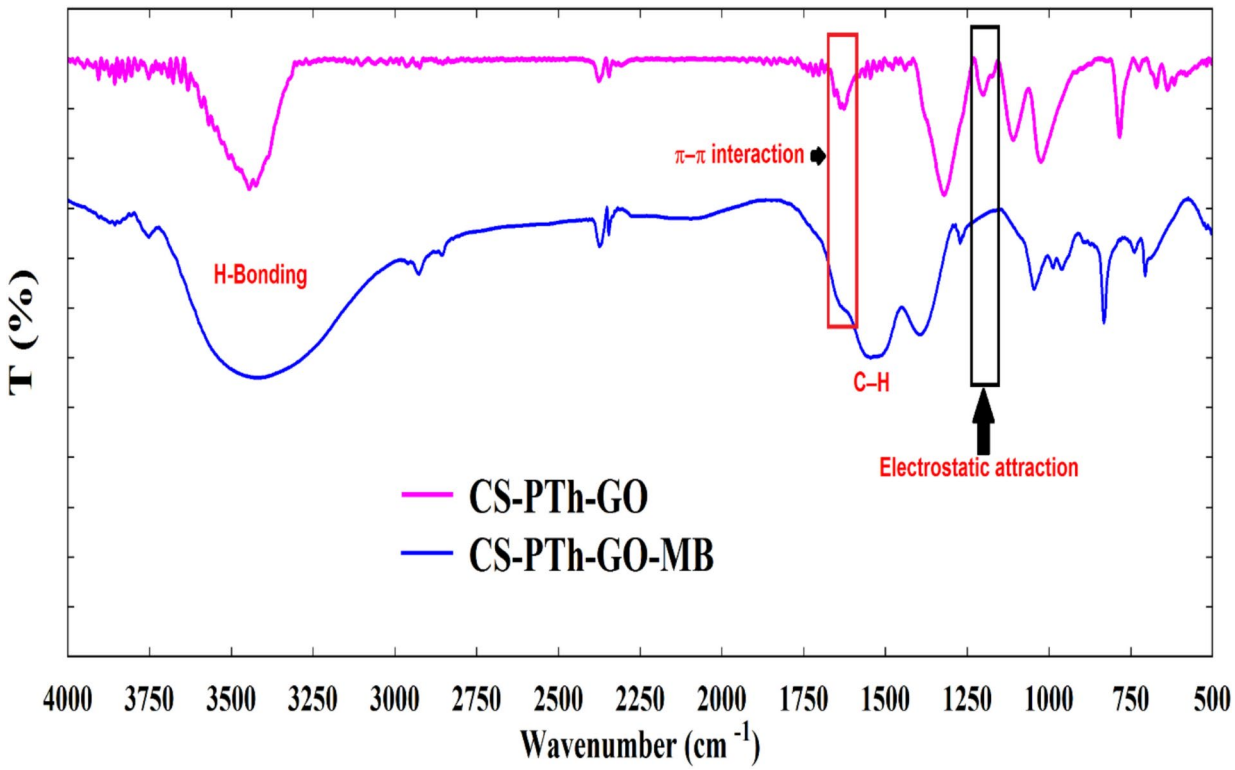

Fig. 10. FTIR of CS–PTh–GO adsorbents before and after MB adsorption.

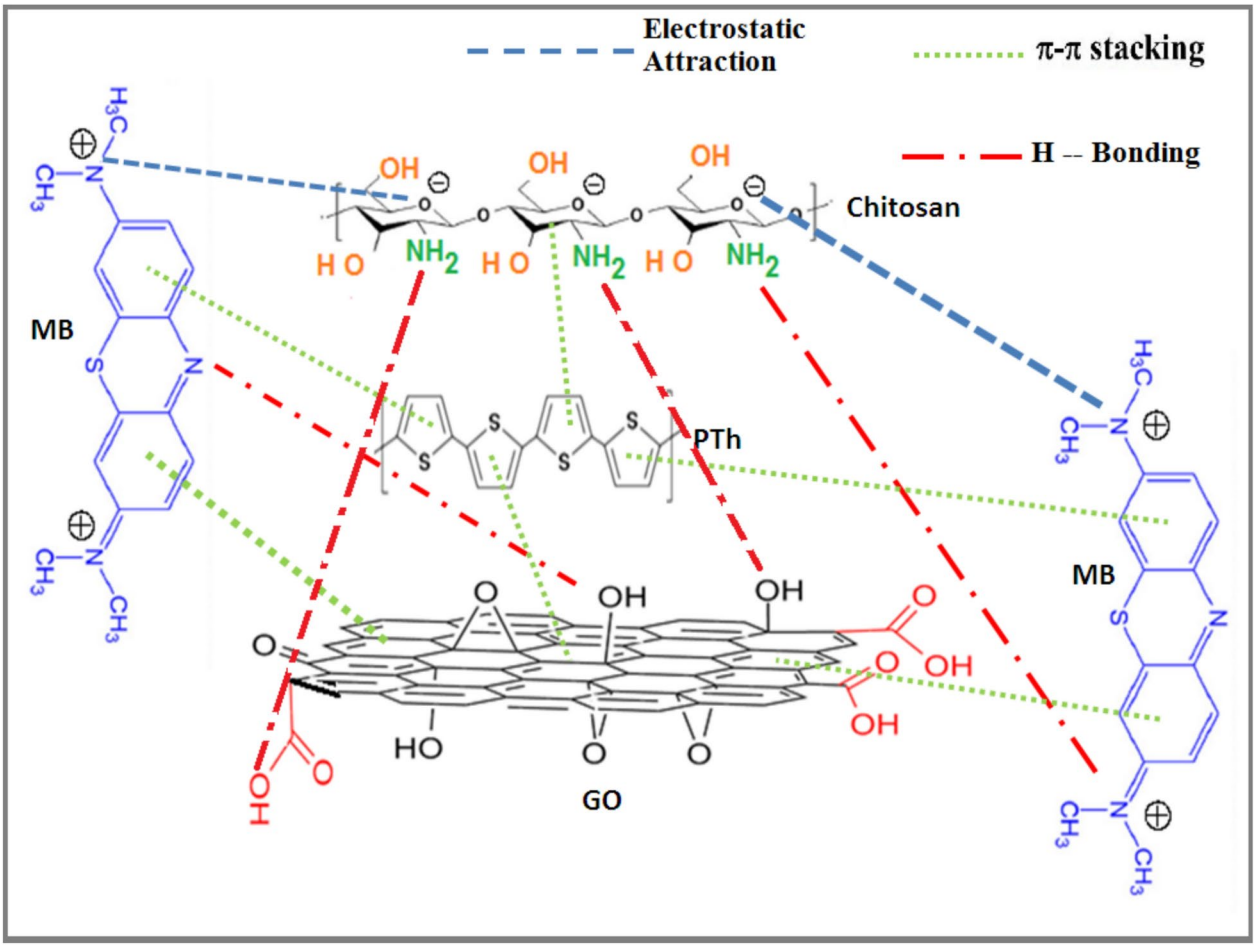

Scheme 2. Schematic illustrations of suggested mechanism for adsorption of MB.

Microorganism	Minimum inhibitory concentration (MIC) (µg/ml)				
	Particles				
	CS–PTh	CS–GO	CS–PTh–GO (PTG1)	CS–PTh–GO (PTG2)	CS–PTh–GO (PTG3)
E. coli	50 ± 3.1	30 ± 2.2	10 ± 2.1	5 ± 1.6	15 ± 2.7
S. aureus	100 ± 4.2	100 ± 3.1	25 ± 2.8	15 ± 2.2	50 ± 1.4
B. Subtilis	200 ± 5.8	150 ± 2.7	50 ± 3.4	50 ± 2.3	100 ± 4.5
C. albicans	25 ± 2.6	15 ± 2.4	5 ± 1.1	2.5 ± 0.5	10 ± 2.3

Table 2. MIC study of CS–PTh–GO bionanocomposites.

Mechanical and thermal properties

Mechanical properties of bionanocomposites were studied using tensile analysis and the results are presented in Fig. 11. Tensile profile of CS has a linear region that is the elastic deformation and a nonlinear characteristic region for plastic strain. From this figure it can be concluded that presence of PTh and GO improved the tensile strength compared to pure CS. In the CS–PTh–GO (PTG2), the mechanical strength improved and reached to 56 MPa that is ~ 70% higher than pure CS. Literature study shows that the dispersion of oriented fillers or functionalized carbon based nanoparticles enhanced the mechanical properties of bionanocomposites[98,99]. The good distribution and interfacial interaction between filler and matrix are the main factors that affected the final properties of nanocomposites as a results of decrease in the stress concentration centers[100,101]. The interactions between GO layers and the CS matrix improved when PTh particles deposited on the GO layers, thus significantly enhanced the mechanical strength of the bionanocomposites. Additionally, the reinforcement effect of GO due to its high aspect ratio and intrinsic stiffness contributes to the superior mechanical properties of the nanocomposite. The tensile analysis shows that (PTG2) has the higher strength and elasticity compared to other CS based nanoocmposites due to the better dispersion of GO in CS matrix in PTG2. In addition to the base CS, the nanocomposite facilitates the creation of an interconnected three-dimensional network

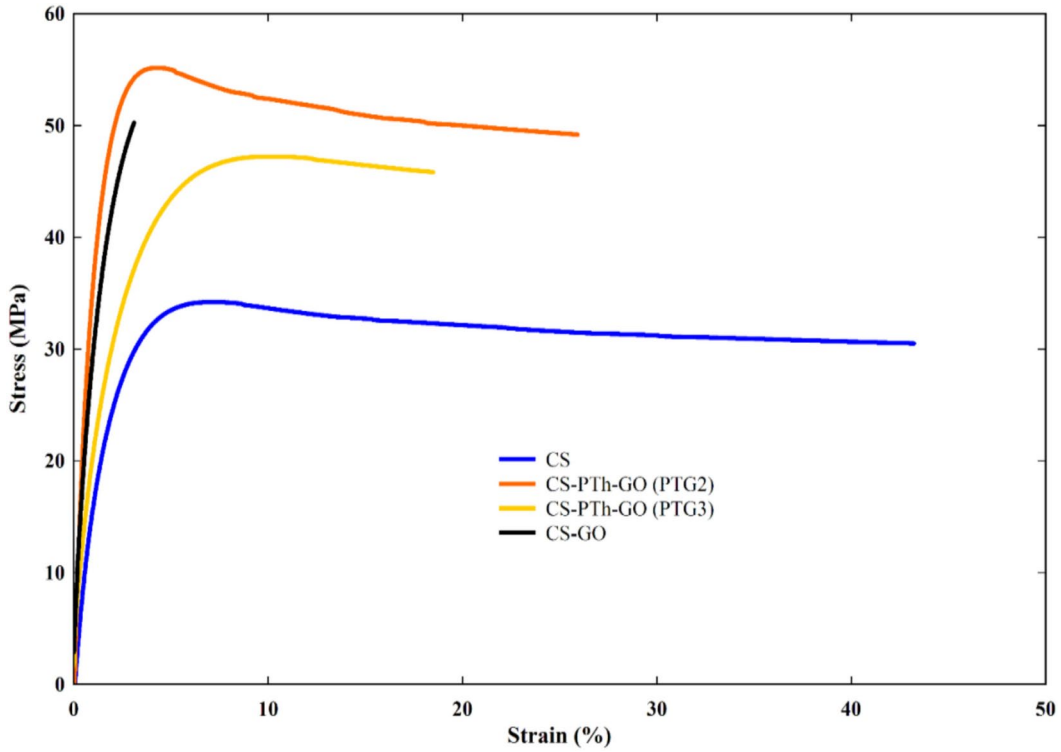

Fig. 11. Tensile properties of CS and the CS based biocomposite.

between the CS matrix and the PTh–GO, leading to an improvement in the mechanical properties of the CS–PTh–GO bionanocomposite. The incorporation of PTh–GO nanocomposite enhances the initial modulus of PTh–GO filled CS nanocomposite due to the hydrodynamic effect. Under tension, the CS matrix undergoes initial deformation, subsequently transferring the load to the rigid network of the PTh–GO embedded within the CS matrix, which facilitates significant energy dissipation through the interfaces of the interconnected 3D network of the CS matrix and the PTh–GO. The CS–PTh–GO bionanocomposite exhibits enhanced elongation without early failure as a result. The enhancement is primarily ascribed to the unique properties of nanoparticles, specifically their substantial surface area to volume ratio and their ability to reinforce the polymer matrix at the nanoscale.

The thermal stability of the bionanocomposites were investigated using thermogravimetric analysis (TGA) and presented in Fig. 12. For CS, 5% weight loss at 100 °C observed as a result of the volatilization water molecules. The main weight loss in the range of 480 °C, related to the decomposition of chitosan backbone, and reached to the 13% residual at 600 °C. The CS–GO and CS–PTh–GO biocomposites have lower decomposition rate and the main weight loss peak observed at around higher than 480 °C[39]. The enhancement in thermal stability in the CS–PTh–GO biocomposite related to the existence of strong interactions between chitosan and GO[102]. The enhancement of the decomposition temperature and residual mass for CS–PTh–GO composites can be explained as follows: (1) the PTh–GO in the CS matrix acted as a radical scavenger, which limited chain cleavage and radical formation and thus mitigated thermal degradation; (2) the PTh–GO forms a gas and heat barrier, the so-called "tortuous path" effect, which prevented the diffusion of volatile decomposed products; and (3) the well-dispersed PTh–GO permitted strong interfacial interactions with the CS matrix through hydrogen bonds, which limited the decomposition of the composites.

Conclusion

A novel bionanocomposite based on chitosan, polythiophene and graphene oxide was synthesized. The CS–PTh–GO bionanocomposites were characterized using FTIR,XRD, SEM, TEM, Tensile, TGA, and antimicrobial activity against bacterial microorganisms. Morphological analysis (XRD, SEM and TEM) confirmed that the incorporation of PTh into the CS–GO had a positive effect on the dispersion of GO throughout the chitosan matrix. Due to the surface roughness of the CS–PTh–GO bionanocomposites, they have great potential for the dye removal from the aques solution. The CS–PTh–GO bionanocomposites showed 97.9% removal of MB in 1.5 h. Moreover, characterization demonstrated that the CS–PTh–GO bionanocomposite has good efficiency for dye removal in the light and dark. The coexistence of PTh and GO within chitosan matrix enhanced the mechanical strength and thermal stability of the CS–PTh–GO bionanocomposites compared to the pure chitosan possibly due to the synergistic effect of PTh, CS and GO and the formation of strong 3D network due to the interactions between PTh and GO with chitosan. The antibacterial analysis showed that CS–PTh–GO exhibited highly effective antibacterial efficacy. Due to the obtained results it can be concluded that the fabricated CS–

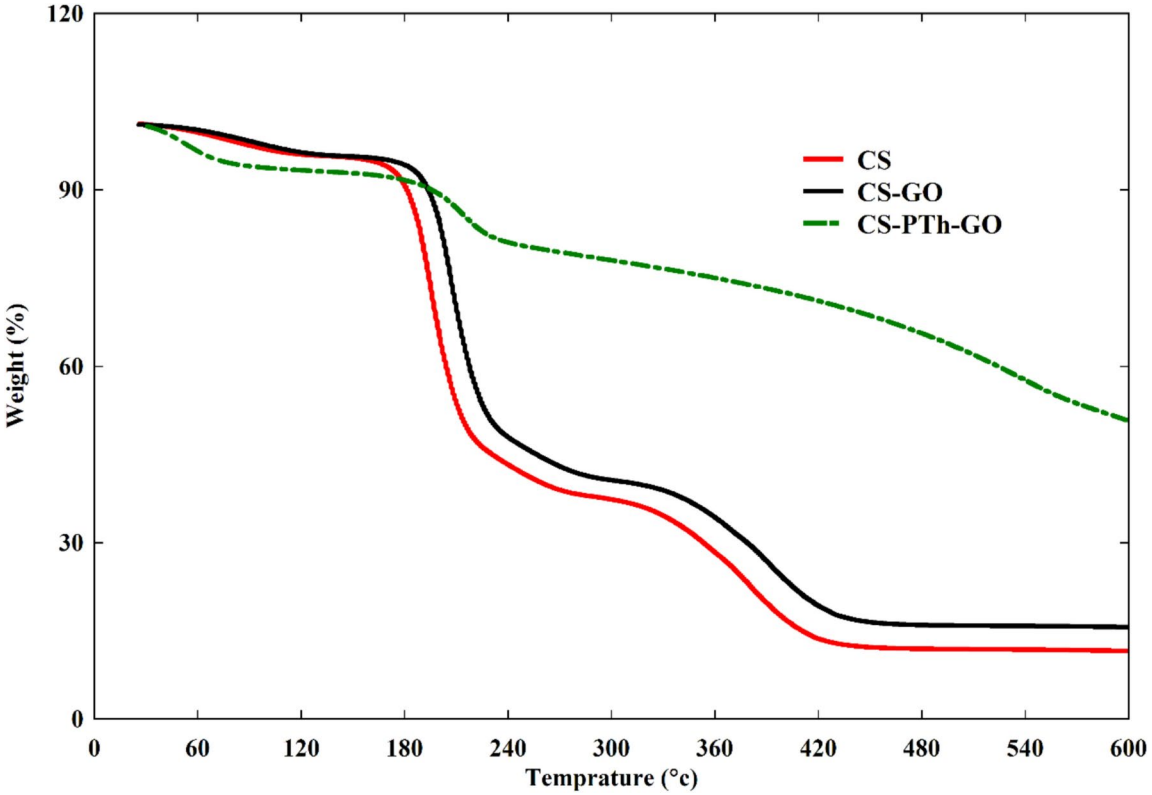

Fig. 12. TGA of CS and the CS based biocomposite.

PTh–GO bionanocomposites can used as a good antibacterial dye absorbent to amend the negative effects of the environment issues.

Data availability

The datasets used and/or analysed during the current study available from the corresponding author on reasonable request.

Received: 9 November 2024; Accepted: 19 March 2025
Published online: 26 March 2025

References

1. Khalil, W. F. et al. Graphene oxide-based nanocomposites (GO-chitosan and GO-EDTA) for outstanding antimicrobial potential against some Candida species and pathogenic bacteria. *Int. J. Biol. Macromol.* **164**, 1370–1383 (2020).
2. Dixit, A., Wazarkar, K. & Sabnis, A. S. Antimicrobial uv curable wood coatings based on citric acid. *Pigment Resin Technol.* **50**, 533–544 (2021).
3. Weisburger, J. H. Comments on the history and importance of aromatic and heterocyclic amines in public health. *Mutat. Res. Fundam. Mol. Mech. Mutagen.* **506–507**, 9–20 (2002).
4. Yang, C. et al. Utilization of powdered peanut hull as biosorbent for removal of anionic dyes from aqueous solution. *Chin. J. Appl. Ecol.* **15**, 2195–2198 (2004).
5. Dutta, P. K. An overview of textile pollution and its remedy. *Indian J. Environ. Prot.* **14**, 443–446 (1994).
6. Benhalima, T., Sadi, A. & Ferfera-Harrar, H. Magnetic adsorbent based on carboxymethyl cellulose for methylene blue uptake from aqueous media. *J. Fundam. Appl. Sci.* **16**, 1–14 (2024).
7. Abu Elella, M. H., Sabaa, M. W., ElHafeez, E. A. & Mohamed, R. R. Crystal violet dye removal using crosslinked grafted xanthan gum. *Int. J. Biol. Macromol.* **137**, 1086–1101 (2019).
8. Ihaddaden, S., Aberkane, D., Boukerroui, A. & Robert, D. Removal of methylene blue (basic dye) by coagulation-flocculation with biomaterials (bentonite and Opuntia ficus indica). *J. Water Process Eng.* **49**, 102952 (2022).
9. Elella, M. H. A., Aamer, N., Mohamed, Y. M. A., El Nazer, H. A. & Mohamed, R. R. Innovation of high-performance adsorbent based on modified gelatin for wastewater treatment. *Polym. Bull.* **79**, 11217–11233 (2022).
10. Abu Elella, M. H. et al. Green antimicrobial adsorbent containing grafted xanthan gum/SiO_2 nanocomposites for malachite green dye. *Int. J. Biol. Macromol.* **191**, 385–395 (2021).
11. Bhatia, D., Sharma, N. R., Singh, J. & Kanwar, R. S. Biological methods for textile dye removal from wastewater: A review. *Crit. Rev. Environ. Sci. Technol.* **47**, 1836–1876 (2017).
12. Sabzehmeidani, M. M., Mahnaee, S., Ghaedi, M., Heidari, H. & Roy, V. A. L. Carbon based materials: A review of adsorbents for inorganic and organic compounds. *Mater. Adv.* **2**, 598–627 (2021).
13. Sharif, M., Heidari, A. & Aghaeinejad Meybodi, A. Polythiophene/zinc oxide/graphene oxide ternary photocatalyst: Synthesis, characterization and application. *Polym. Technol. Mater.* **60**, 1450–1460 (2021).
14. Mohammadzadeh Pakdel, P. & Peighambardoust, S. J. Review on recent progress in chitosan-based hydrogels for wastewater treatment application. *Carbohydr. Polym.* **201**, 264–279 (2018).

15. Kahya, N. & Erim, F. B. Graphene oxide/chitosan-based composite materials as adsorbents in dye removal. *Chem. Eng. Commun.* **209**, 1711–1726 (2022).
16. Silva, A. O., Cunha, R. S., Hotza, D. & Machado, R. A. F. Chitosan as a matrix of nanocomposites: A review on nanostructures, processes, properties, and applications. *Carbohydr. Polym.* **272**, 118472 (2021).
17. de Brião, G. V., de Andrade, J. R., da Silva, M. G. C. & Vieira, M. G. A. Removal of toxic metals from water using chitosan-based magnetic adsorbents. A review. *Environ. Chem. Lett.* **18**, 1145–1168 (2020).
18. Sharif, M. & Tavakoli, S. Biodegradable chitosan–graphene oxide as an affective green filler for improving of properties in epoxy nanocomposites. *Int. J. Biol. Macromol.* **233**, 123550 (2023).
19. Sharif, M. & Tavakoli, S. Chitosan-modified graphene oxide filled photo-curable nanocomposite coating with advanced properties. *Polym. Bull.* **81**, 11481–11498 (2024).
20. Abu Elella, M. H., Abdallah, H. M., Gamal, H., Moustafa, E. B. & Goda, E. S. Rational design of biocompatible IPNs hydrogels containing carboxymethyl starch and trimethyl chitosan chloride with high antibacterial activity. *Cellulose* **29**, 7317–7330 (2022).
21. Wegrzynowska-Drzymalska, K. et al. Crosslinking of chitosan with dialdehyde chitosan as a new approach for biomedical applications. *Materials (Basel)* **13**, 1–27 (2020).
22. Elella, M. H. A., Aamer, N., Mohamed, Y. M. A., Nazer, H. A. E. & Mohamed, R. R. High-potential removal of copper (II) ions from aqueous solution using antimicrobial crosslinked grafted Gelatin hydrogels. *J. Polym. Environ.* **31**, 1071–1089 (2023).
23. Chen, S. et al. Photodynamic antibacterial chitosan/nitrogen-doped carbon dots composite packaging film for food preservation applications. *Carbohydr. Polym.* **314**, 120938 (2023).
24. Atay, H. Y. Antibacterial activity of chitosan-based systems. *Funct. Chitosan Drug Deliv. Biomed. Appl.* https://doi.org/10.1007/978-981-15-0263-7_15 (2020).
25. Priyadarshi, G., Raval, N. P. & Trivedi, M. H. Microwave-assisted synthesis of cross-linked chitosan-metal oxide nanocomposite for methyl orange dye removal from unary and complex effluent matrices. *Int. J. Biol. Macromol.* **219**, 53–67 (2022).
26. Zang, X. et al. A review on the progress of magnetic chitosan-based materials in water purification and solid-phase extraction of contaminants. *Sep. Purif. Technol.* **330**, 125521 (2024).
27. Li, L. et al. Biodegradable and injectable in situ cross-linking chitosan-hyaluronic acid based hydrogels for postoperative adhesion prevention. *Biomaterials* **35**, 3903–3917 (2014).
28. El-Fattah, M. A., El Saeed, A. M., Azzam, A. M., Abdul-Raheim, A. R. M. & Hefni, H. H. H. Improvement of corrosion resistance, antimicrobial activity, mechanical and chemical properties of epoxy coating by loading chitosan as a natural renewable resource. *Prog. Org. Coat.* **101**, 288–296 (2016).
29. Zhou, W. et al. Collagen-modified chitosan microsphere as a novel hemoperfusion adsorbent for efficient removal of bilirubin from human plasma. *Sep. Purif. Technol.* **337**, 126303 (2024).
30. Chang, Y. et al. In vitro toxicity evaluation of graphene oxide on A549 cells. *Toxicol. Lett.* **200**, 201–210 (2011).
31. Saleh, R. & Taufik, A. Degradation of methylene blue and congo-red dyes using Fenton, photo-Fenton, sono-Fenton, and sonophoto-Fenton methods in the presence of iron(II, III) oxide/zinc oxide/graphene (Fe3O4/ZnO/graphene) composites. *Sep. Purif. Technol.* **210**, 563–573 (2019).
32. Ferfera-Harrar, H., Benhalima, T. & Lerari, D. Sustainable hydrogel nanocomposites based on grafted chitosan and clay for effective adsorption of cationic dye. *Int. J. Mater. Metall. Eng.* **14**, 5–15 (2020).
33. Motshabi, B. R. et al. Synthesis of locust bean gum/titanium dioxide hydrogel nanocomposites for efficient removal of methylene blue from aqueous solution. *J. Polym. Environ.* https://doi.org/10.1007/s10924-024-03237-1 (2024).
34. Benhalima, T., Ferfera-Harrar, H., Doufene, N. & Sadi, A. Silver decorated zeolite embedded in bionanocomposite hydrogels based on cross-linked carboxymethyl cellulose for excellent catalytic hydrogenation of azo dyes. *Int. J. Biol. Macromol.* **279**, 135556 (2024).
35. Benhalima, T., Sadi, A., Dairi, N. & Ferfera-Harrar, H. Multifunctional carboxymethyl cellulose-dextran sulfate/AgNPs@zeolite hydrogel beads for basic red 46 and methylene blue dyes removal and water disinfection control. *Sep. Purif. Technol.* **342**, 127001 (2024).
36. Abu Elella, M. H. et al. Novel high-efficient adsorbent based on modified gelatin/montmorillonite nanocomposite for removal of malachite green dye. *Sci. Rep.* **14**, 1228 (2024).
37. Ferfera-Harrar, H., Sadi, A. & Benhalima, T. Magnetic recyclable carboxymethyl cellulose/gelatin/citrate@Fe3O4 photo-nanocomposite beads for ciprofloxacin removal via hybrid adsorption/photocatalysis process under solar light as a renewable energy source. *Int. J. Biol. Macromol.* **282**, 136854 (2024).
38. Gandomkar, A. & Sharif, M. Nano composites performance as direct thickeners for gas based enhanced oil recovery, a new approach. *J. Pet. Sci. Eng.* **194**, 107491 (2020).
39. Khezri, T., Sharif, M. & Pourabas, B. Polythiophene-graphene oxide doped epoxy resin nanocomposites with enhanced electrical, mechanical and thermal properties. *RSC Adv.* **6**, 93680–93693 (2016).
40. Sharif, M. & Pourabas, B. Enhancement of electrical and mechanical properties of su-8 photocrosslinked coatings containing polypyrrole-graphene oxide nanoparticles. *J. Photopolym. Sci. Technol.* **29**, 787–791 (2016).
41. Liu, S. et al. Antibacterial activity of graphite, graphite oxide, graphene oxide, and reduced graphene oxide: Membrane and oxidative stress. *ACS Nano* **5**, 6971–6980 (2011).
42. Shah, I. A., Bilal, M., Almanassra, I. W. & Ihsanullah, I. A comprehensive review of graphene oxide-based membranes for efficient dye removal from water sources. *Sep. Purif. Technol.* **330**, 125277 (2024).
43. Chen, W. L., Cheng, C. C., Lu, C. H. & Chen, J. K. Fabrication of sandwich-structured capacitor containing core@shell polystyrene@graphene oxide microspheres for switchable removal of dyes from water by dielectrophoresis force. *Sep. Purif. Technol.* **331**, 125600 (2024).
44. Hu, W. et al. Graphene-based antibacterial paper. *ACS Nano* **4**, 4317–4323 (2010).
45. Akhavan, O. & Ghaderi, E. Toxicity of graphene and graphene oxide nanowalls against bacteria. *ACS Nano* **4**, 5731–5736 (2010).
46. Shi, Y. et al. Graphene oxide-chitosan composite aerogel for adsorption of methyl orange and methylene blue: Effect of pH in single and binary systems. *Colloids Surfaces A Physicochem. Eng. Asp.* **641**, 128595 (2022).
47. Sabzevari, M., Cree, D. E. & Wilson, L. D. Graphene oxide-chitosan composite material for treatment of a model dye effluent. *ACS Omega* **3**, 13045–13054 (2018).
48. Yan, D. et al. Antimicrobial properties of chitosan and chitosan derivatives in the treatment of enteric infections. *Molecules* **26**, 7136 (2021).
49. Naveen, M. H., Gurudatt, N. G. & Shim, Y. B. Applications of conducting polymer composites to electrochemical sensors: A review. *Appl. Mater. Today* **9**, 419–433 (2017).
50. Nezakati, T., Seifalian, A., Tan, A. & Seifalian, A. M. Conductive polymers: Opportunities and challenges in biomedical applications. *Chem. Rev.* **118**, 6766–6843 (2018).
51. Moosaei, R., Sharif, M. & Ramezannezhad, A. Enhancement of tensile, electrical and thermal properties of epoxy nanocomposites through chemical hybridization of polypyrrole and graphene oxide. *Polym. Test.* **60**, 173–186 (2017).
52. Roncali, J. Conjugated poly(thiophenes): Synthesis, functionalization, and applications. *Chem. Rev.* **92**, 711–738 (1992).
53. Murugavel, S. & Malathi, M. Structural, photoconductivity, and dielectric studies of polythiophene-tin oxide nanocomposites. *Mater. Res. Bull.* **81**, 93–100 (2016).
54. Kaloni, T. P., Giesbrecht, P. K., Schreckenbach, G. & Freund, M. S. Polythiophene: From fundamental perspectives to applications. *Chem. Mater.* **29**, 10248–10283 (2017).

55. Muliwa, A. M., Onyango, M. S., Maity, A. & Ochieng, A. Batch equilibrium and kinetics of mercury removal from aqueous solutions using polythiophene/graphene oxide nanocomposite. *Water Sci. Technol.* **75**, 2841–2851 (2017).
56. Bazireh, E. & Sharif, M. Polythiophene-coated multi-walled carbon nanotube-reinforced epoxy nanocomposites for enhanced mechanical, electrical and thermal properties. *Polym. Bull.* **77**, 4537–4553 (2020).
57. Ray, S. S., Gusain, R. & Kumar, N. Conducting polymer-functionalized carbon nanomaterials-based adsorbents. *Carbon Nanomater. Adsorbents Water Purif.* https://doi.org/10.1016/b978-0-12-821959-1.00013-1 (2020).
58. Mehdinia, A., Khodaee, N. & Jabbari, A. Fabrication of graphene/Fe_3O_4@polythiophene nanocomposite and its application in the magnetic solid-phase extraction of polycyclic aromatic hydrocarbons from environmental water samples. *Anal. Chim. Acta* **868**, 1–9 (2015).
59. Mir, A., Fletcher, W. J., Taylor, D. K., Alam, J. & Riaz, U. sustained release studies of metformin hydrochloride drug using conducting polymer/gelatin-based composite hydrogels. *ACS Omega* **9**, 18766–18776 (2024).
60. Myrick, S. et al. Graphene oxide-modified polythiophene nanohybrids: Antibacterial properties and sonophotocatalytic degradation of dyes under visible-light irradiation. *Int. J. Polym. Mater. Polym. Biomater.* **73**, 1451–1460 (2024).
61. Benhalima, T., Mokhtari, M. & Ferfera-Harrar, H. Synergistic adsorption/photodegradation effect for effective removal of crystal violet dye and acetamiprid pesticide using Fe3+ cross-linked ternary carboxymethyl cellulose/polyaniline/TiO_2 photocomposites. *J. Water Process Eng.* **57**, 104670 (2024).
62. Shahabuddin, S., Sarih, N. M., Ismail, F. H., Shahid, M. M. & Huang, N. M. Synthesis of chitosan grafted-polyaniline/Co_3O_4 nanocube nanocomposites and their photocatalytic activity toward methylene blue dye degradation. *RSC Adv.* **5**, 83857–83867 (2015).
63. Herrera, M. U., Futalan, C. M., Gapusan, R. & Balela, M. D. L. Removal of methyl orange dye and copper (II) ions from aqueous solution using polyaniline-coated kapok (Ceiba pentandra) fibers. *Water Sci. Technol.* **78**, 1137–1147 (2018).
64. Mohammadi, B., Pirsa, S. & Alizadeh, M. Preparing chitosan–polyaniline nanocomposite film and examining its mechanical, electrical, and antimicrobial properties. *Polym. Polym. Compos.* **27**, 507–517 (2019).
65. Pasela, B. R. et al. Synthesis and characterization of acetic acid-doped polyaniline and polyaniline-chitosan composite. *Biomimetics* **4**, 15 (2019).
66. Moutsatsou, P., Coopman, K. & Georgiadou, S. Chitosan & conductive PANI/chitosan composite nanofibers: Evaluation of antibacterial properties. *Curr. Nanomater.* **4**, 6–20 (2018).
67. Pandiselvi, K. & Thambidurai, S. Synthesis of adsorption cum photocatalytic nature of polyaniline-ZnO/chitosan composite for removal of textile dyes. *Desalin. Water Treat.* **57**, 8343–8357 (2016).
68. Zare, M., Sharif, M. & Kashkooli, A. Study on the effect of polypyrrole and polypyrrole/graphene oxide nanoparticles on the microstructure, electrical and tensile properties of polypropylene nanocomposites. *Polym. - Plast. Technol. Eng.* **53**, 1392–1401 (2014).
69. Bahrani, M., Sharif, M. & Amirazodi, K. Preparation and characterization of polythiophene/graphene oxide/epoxy nanocomposite coatings with advanced properties. *Polym. Bull.* **79**, 263–284 (2022).
70. Sanmugam, A., Vikraman, D., Park, H. J. & Kim, H. S. One-pot facile methodology to synthesize chitosan-ZnO-graphene oxide hybrid composites for better dye adsorption and antibacterial activity. *Nanomaterials* **7**, 363 (2017).
71. Amruth, K., Abhirami, K. M., Sankar, S. & Ramesan, M. T. Synthesis, characterization, dielectric properties and gas sensing application of polythiophene/chitosan nanocomposites. *Inorg. Chem. Commun.* **136**, 109184 (2022).
72. Revathi, T. & Thambidurai, S. Synthesis of chitosan incorporated neem seed extract (Azadirachta indica) for medical textiles. *Int. J. Biol. Macromol.* **104**, 1890–1896 (2017).
73. El-Shahawy, A. A. G., Zohery, M. & El-Dek, S. I. Theranostics platform of Abemaciclib using magnetite@silica@chitosan nanocomposite. *Int. J. Biol. Macromol.* **221**, 634–643 (2022).
74. Zhang, Y., Deng, X., Wang, L. & Wei, T. Inclusion compounds formation of poly(azomethine ether)s and β-cyclodextrin. *J. Macromol. Sci. Part A Pure Appl. Chem.* **45**, 289–294 (2008).
75. Yang, X., Tu, Y., Li, L., Shang, S. & Tao, X. M. Well-dispersed chitosan/graphene oxide nanocomposites. *ACS Appl. Mater. Interfaces* **2**, 1707–1713 (2010).
76. Qiu, B. et al. Construction of chitosan/ZnO nanocomposite film by in situ precipitation. *Int. J. Biol. Macromol.* **122**, 82–87 (2019).
77. Azimi, N., Gandomkar, A. & Sharif, M. Relationship between production condition, microstructure and final properties of chitosan/graphene oxide–zinc oxide bionanocomposite. *Polym. Bull.* https://doi.org/10.1007/s00289-022-04277-0 (2022).
78. Rahmatpour, A., Alijani, N. & Alizadeh, A. H. Preparation of chitosan-based ternary nanocomposite hydrogel film by loading graphene oxide nanosheets as adsorbent for enhanced methylene blue dye removal. *Int. J. Biol. Macromol.* **253**, 126585 (2023).
79. Hussain, D., Siddiqui, M. F. & Khan, T. A. Preparation of $NiFe_2O_4$/polythiophene nanocomposite and its enhanced adsorptive uptake of Janus green B and Fuchsin basic from aqueous solution: Isotherm and kinetics studies. *Environ. Prog. Sustain. Energy* https://doi.org/10.1002/ep.13371 (2020).
80. Ali, M. E. A. Synthesis and adsorption properties of chitosan-CDTA-GO nanocomposite for removal of hexavalent chromium from aqueous solutions. *Arab. J. Chem.* **11**, 1107–1116 (2018).
81. Hameed, B. H. Equilibrium and kinetic studies of methyl violet sorption by agricultural waste. *J. Hazard. Mater.* **154**, 204–212 (2008).
82. Abdul Mubarak, N. S., Bahrudin, N. N., Jawad, A. H., Hameed, B. H. & Sabar, S. Microwave enhanced synthesis of sulfonated chitosan-montmorillonite for effective removal of methylene blue. *J. Polym. Environ.* **29**, 4027–4039 (2021).
83. Mashkoor, F., Nasar, A. & Jeong, C. Magnetized chitosan nanocomposite as an effective adsorbent for the removal of methylene blue and malachite green dyes. *Biomass Convers. Biorefinery* **14**, 313–325 (2024).
84. Kaur, K. & Jindal, R. Self-assembled GO incorporated CMC and Chitosan-based nanocomposites in the removal of cationic dyes. *Carbohydr. Polym.* **225**, 115245 (2019).
85. Wang, J. et al. Reduced graphene oxide/ZnO composite: Reusable adsorbent for pollutant management. *ACS Appl. Mater. Interfaces* **4**, 3084–3090 (2012).
86. Pourjavadi, A., Nazari, M. & Hosseini, S. H. Synthesis of magnetic graphene oxide-containing nanocomposite hydrogels for adsorption of crystal violet from aqueous solution. *RSC Adv.* **5**, 32263–32271 (2015).
87. Alqadami, A. A., Naushad, M., Alothman, Z. A. & Ahamad, T. Adsorptive performance of MOF nanocomposite for methylene blue and malachite green dyes: Kinetics, isotherm and mechanism. *J. Environ. Manage.* **223**, 29–36 (2018).
88. Rostamian, M. et al. Introducing a bio sorbent for removal of methylene blue dye based on flexible poly(glycerol sebacate)/chitosan/graphene oxide ecofriendly nanocomposites. *Chemosphere* **289**, 133219 (2022).
89. Minisy, I. M., Salahuddin, N. A. & Ayad, M. M. Adsorption of methylene blue onto chitosan–montmorillonite/polyaniline nanocomposite. *Appl. Clay Sci.* **203**, 105993 (2021).
90. El-Sharkaway, E. A., Kamel, R. M., El-Sherbiny, I. M. & Gharib, S. S. Removal of methylene blue from aqueous solutions using polyaniline/graphene oxide or polyaniline/reduced graphene oxide composites. *Environ. Technol. (United Kingdom)* **41**, 2854–2862 (2020).
91. Duhan, M. & Kaur, R. Phytic acid doped polyaniline nanofibers: An advanced adsorbent for methylene blue dye. *Environ. Nanotechnol. Monit. Manag.* **12**, 100248 (2019).
92. Taha, G. M., Mansor, E. S. & Sultan, M. Development of Arabic gum-based $AgTiO_2$ nanocomposite hydrogel as high efficient adsorbent of cationic dye methylene blue from water. *Int. J. Biol. Macromol.* **193**, 1859–1870 (2021).

93. Thakur, S., Pandey, S. & Arotiba, O. A. Development of a sodium alginate-based organic/inorganic superabsorbent composite hydrogel for adsorption of methylene blue. *Carbohydr. Polym.* **153**, 34–46 (2016).
94. Nasaj, M. et al. Factors influencing the antimicrobial mechanism of chitosan action and its derivatives: A review. *Int. J. Biol. Macromol.* **277**, 134321 (2024).
95. Shan, Z. et al. Hollow dodecahedra graphene oxide- cuprous oxide nanocomposites with effective photocatalytic and bactericidal activity. *Front. Chem.* https://doi.org/10.3389/fchem.2021.755836 (2021).
96. Nanda, S. S., Yi, D. K. & Kim, K. Study of antibacterial mechanism of graphene oxide using Raman spectroscopy. *Sci. Rep.* **6**, 28443 (2016).
97. Zhang, L. et al. Ten-Gram-scale mechanochemical synthesis of ternary lanthanum coordination polymers for antibacterial and antitumor activities. *Front. Chem.* **10**, 898324 (2022).
98. Gorga, R. E. & Cohen, R. E. Toughness enhancements in poly(methyl methacrylate) by addition of oriented multiwall carbon nanotubes. *J. Polym. Sci. Part B Polym. Phys.* **42**, 2690–2702 (2004).
99. Wang, Z. & Li, X. Mechanical properties and flame retardancy of rigid polyurethane foams containing SiO_2 Nanospheres/Graphene Oxide Hybrid and Dimethyl methylphosphonate. *Polym.: Plast. Technol. Eng.* **57**, 884–892 (2018).
100. Han, D., Yan, L., Chen, W. & Li, W. Preparation of chitosan/graphene oxide composite film with enhanced mechanical strength in the wet state. *Carbohydr. Polym.* **83**, 653–658 (2011).
101. Wu, L. et al. Fabrication of multifunctional carbon/clay nanocomposites by recycling oil shale semi-coke waste for coloring and enhancing mechanical and aging-resistant properties of acrylonitrile–butadiene–styrene. *Mater. Today Sustain.* **20**, 100259 (2022).
102. Ren, Y. et al. Grafting natural nicotinamide on tempo-oxidized cellulose nanofibrils to prepare flexible and transparent nanocomposite films with fascinating mechanical strength and UV shielding performance. *Int. J. Biol. Macromol.* https://doi.org/10.1016/j.ijbiomac.2022.10.148 (2022).

Author contributions

Mohammad Amin Sedghamiz: Conceptualization, Methodology, Formal analysis. Mehdi Sharif: Conceptualization, Methodology, Formal analysis, Investigation, Writing—original draft, Writing—review and editing. Mohammadhadi Mehrvar: Writing—review and editing. Mohammad Amin Tavakkoli: Methodology, Formal analysis, Investigation, Writing—original draft. Mehdi Sahami: Investigation, Writing & editing.

Declarations

Competing interests

The authors declare no competing interests.

Additional information

Correspondence and requests for materials should be addressed to M.A.S. or M.S.

Reprints and permissions information is available at www.nature.com/reprints.

Publisher's note Springer Nature remains neutral with regard to jurisdictional claims in published maps and institutional affiliations.